Complex exchange mechanism driven ferromagnetism in half-metallic Heusler Co₂TiGe: Evidence from critical behavior

Shubhankar Roy,[1,2] Nazir Khan,[1] Ratnadwip Singha,[1] Arnab Pariari,[1] and Prabhat Mandal[1]

[1]*Saha Institute of Nuclear Physics, HBNI, 1/AF Bidhannagar, Kolkata 700 064, India*
[2]*Vidyasagar Evening College, 39, Sankar Ghosh Lane, Kolkata 700 006, India*

We have investigated the critical phenomenon associated with the magnetic phase transition in the half-metallic full-Heusler Co₂TiGe. The compound undergoes a continuous paramagnetic-to-ferromagnetic phase transition below the Curie temperature $T_C = 371.5$ K. The analysis of magnetization isotherms in the vicinity of T_C, following a modified Arrott plot method, the Kouvel-Fisher technique, and a critical isotherm plot, yields the asymptotic critical exponents $\beta = 0.495$, $\gamma = 1.324$, and $\delta = 3.67$. The self-consistency and reliability of the obtained exponents are further verified by the Widom scaling relation and scaling equations of state. The mean-field-like value of the critical exponent β suggests a long-range nature of the exchange interactions, whereas the values of the critical exponents γ and δ imply sizable critical spin fluctuations. The half-metallic itinerant character of Co₂TiGe in the presence of magnetic inhomogeneity may result in such a strong deviation from the three-dimensional Heisenberg values ($\beta = 0.369$, $\gamma = 1.38$, and $\delta = 4.8$) of the critical exponents toward the mean-field values ($\beta = 0.5$, $\gamma = 1$, and $\delta = 3$). The results suggest the complex nature of exchange couplings that stabilize the long-range ferromagnetic ordering in the system and are consistent with the earlier theoretical studies on the exchange mechanism in Co₂TiGe.

I. INTRODUCTION

The discovery of ferromagnetism by Heusler in Cu₂MnAl, which does not contain any of the pure ferromagnetic elements, initiated an ever-growing research interest in intermetallic compounds [1]. Subsequently, numerous experimental works [2–4] have been carried out and several theoretical models [5–11] have been proposed to understand the microscopic interactions that lead to the long-range magnetic ordering in this class of materials. The fascinating half-metallic character [12,13] makes them very promising candidates for spintronics applications at room temperature [14]. Moreover, novel topological semimetal states have been discovered recently in these systems [15]. The Co₂-based ternary intermetallic Heusler compounds, viz., Co₂$M'Z$, where M' is a transition metal and Z is a main group element, received special interest and became the most widely studied systems because of their very high Curie temperatures [11].

Co₂TiGe crystallizes in cubic $L2_1$ structure (space group: $Fm\bar{3}m$), which consists of four interpenetrating face-centered-cubic (fcc) lattices. The crystallographic positions of Co atoms are (0,0,0) and (1/2,1/2,1/2), and those of the Ti and Ge atoms are (1/4,1/4,1/4) and (3/4,3/4,3/4), respectively. There are several theoretical and experimental reports on the structural, electronic, and magnetic properties of Co₂TiGe [16]. Spin-resolved band-structure calculations show that the majority spin-band has a metallic character, whereas the minority spin-band exhibits semiconducting behavior with a band gap of about 0.5 eV at the Fermi level [15,16]. Further, the inclusion of spin-orbit coupling (SOC), albeit very weak, in the band-structure calculation reveals a novel topological Weyl semimetal state [15]. The temperature dependence of the

resistivity of Co₂TiGe shows typical metallic behavior down to 2 K [16]. The origin of ferromagnetism in half-metallic Co₂-based Heusler alloys is a rather complicated issue and remains one of the most interesting problems in modern magnetism. They exhibit Slater-Pauling-type behavior for the magnetization, where the saturation magnetization scales with the total number of valance electrons in the unit cell, leading to a characteristic integer magnetic moment. Magnetic Heusler alloys are traditionally believed to be ideal local-moment systems [17], and their exchange couplings can be described by a Heisenberg Hamiltonian. However, several theoretical reports claim the presence of complex exchange interactions of the localized magnetic moments in these Heusler compounds [6,8–11]. Both the short-range direct exchange coupling between the nearest-neighbor spins and the coupling between further neighbor spins mediated by the Ruderman-Kittel-Kasuya-Yosida (RKKY) -type long-range interaction are believed to be responsible for the long-range magnetic ordering [11]. It is concluded that intersublattice and intrasublattice exchange interactions of different strength stabilize robust ferromagnetic ordering with remarkably high Curie temperatures in these compounds. However, a recent theoretical study shows that in the Co₂TiZ system, the magnetic moment of the Co atoms and that of the Ti atoms are not completely localized, which is further supported by the disordered local-moment calculation [16]. Thus, the presence of a localized magnetic moment is not a prerequisite for the occurrence of half-metallic ferromagnetism. Furthermore, significant orbital magnetic moments in different Co₂$M'Z$ compounds as probed by x-ray magnetic circular dichroism studies [17–19] indicate that the SOC may result in magnetocrystalline anisotropy.
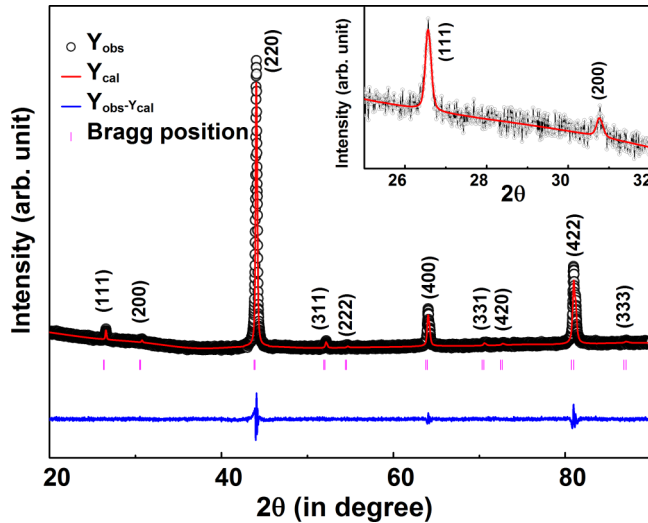
FIG. 1. Rietveld profile refinement of the XRD pattern of powdered samples of Co_2TiGe. The black circles are experimental data (Y_{obs}), the red line is the calculated pattern (Y_{cal}), the blue line is the difference between experimental and calculated intensities ($Y_{obs} - Y_{cal}$), and the magenta vertical lines show the Bragg positions. The inset shows clearly the presence of (111) and (200) superlattice reflections in Co_2TiGe.

FIG. 2. Field dependence of the magnetization (M vs H) at 2 K. Right inset: temperature dependence of the magnetization (M vs T) measured at 500 Oe. Left inset: dM/dT vs temperature.

So, anisotropic exchange interaction may also be involved in the magnetic ordering phenomenon in these systems. The values of the critical exponents associated with a continuous magnetic phase transition reflect the nature of the exchange mechanism, the spin symmetry, or the magnetic anisotropy, and the effective dimensionality of spin-spin interactions in the system [20]. Therefore, by investigating the critical phenomenon associated with the ferromagnetic-to-paramagnetic (FM-to-PM) phase transition in Co_2TiGe, we have tried to clarify different aspects of the exchange mechanism in the Co_2-based Heusler alloy.

II. EXPERIMENTAL DETAILS

The Co_2TiGe compound was prepared by arc-melting stoichiometric amounts of its constituents in a highly purified argon atmosphere. The obtained ingots were then sealed in an evacuated quartz tube and annealed for about 3 weeks. Phase purity and a structural analysis of the sample were done using the powder x-ray diffraction (XRD) technique with Cu $K\alpha$ radiation in a Rigaku x-ray diffractometer (TTRAX III). The Rietveld profile refinement of the XRD pattern (Fig. 1) shows that the compound is single-phase in nature. The presence of weak (111) and (200) superlattice reflections (Fig. 1, inset) indicates that this material orders in $L2_1$-type structure with $Fm\bar{3}m$ space group and is consistent with earlier reports [16,21]. However, these peaks, in particular (200), are much weaker as compared to that reported for Co_2TiSi and Co_2TiSn [16,21]. This is due to the nearly equal scattering factors of Co, Ti, and Ge, which are from the same row in the Periodic Table [22]. The complete absence of the (200) peak might indicate structural disorder [23]. In such cases, an unambiguous determination of the true structure by refining the XRD pattern could be very difficult and may
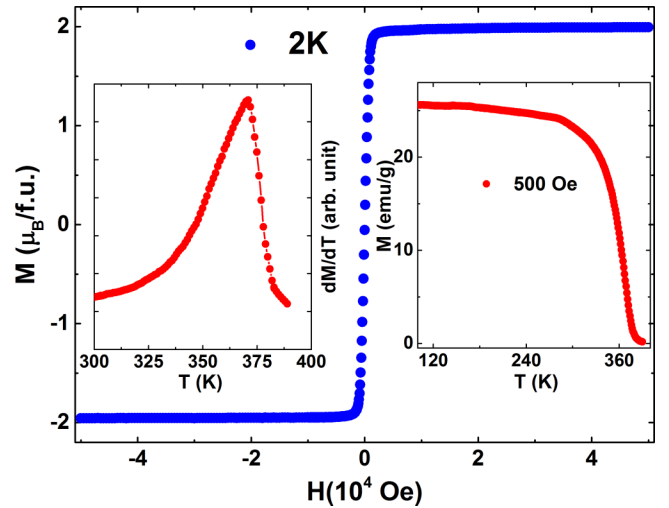
require additional experimental techniques [16,24]. The refined lattice parameters, $a = b = c = 5.811(1)$Å, are in good agreement with that reported previously [16,25]. The magnetization measurements were done using a superconducting quantum interference device–vibrating sample magnetometer (SQUID-VSM) (MPMS 3, Quantum Design) in fields up to 5 T. The sample used for the magnetic measurements is of approximate dimensions $0.5 \times 0.5 \times 4$ mm^3. To minimize the demagnetization effect, the external magnetic field was applied along the longest sample direction. The magnetization data were recorded over the temperature range from 366 to 377 K at 1.0 K intervals. To achieve good thermal equilibrium, we have stabilized each temperature for 45 min. For each $M(H)$ isotherm, the magnetic field was increased from 0 to 5 T and then reduced to 0. We did not find any difference in $M(H)$ between the increasing and decreasing field.

III. RESULTS AND DISCUSSIONS

Figure 2 shows the magnetic-field dependence of dc magnetization (M) at 2 K. In the right inset of Fig. 2, we have plotted M as a function of temperature, measured at 500 Oe. The observed behavior is quite similar to the earlier reports [16,25]. As mentioned before, the Co-based Heusler alloys, which are half-metallic ferromagnets (FMs), exhibit the Slater-Pauling-type behavior of the magnetization as given by $M_p = (Z_p - 24)\mu_B$/f.u. Here, M_p is the total magnetic moment and Z_p is the total number of valence electrons in the unit cell of the compound. For Co_2TiGe, the value of Z_p is 26. Therefore, according to the above relation, the total magnetic moment should be $2\mu_B$/f.u. From Fig. 2, the saturation magnetization is estimated to be $\sim 1.99\mu_B$/f.u., which implies that the compound obeys the Slater-Pauling rule. As shown in the inset of Fig. 2, the magnetization curve mimics a continuous or second-order FM-to-PM phase transition. From the temperature derivative of this magnetization curve (left inset of Fig. 2), the Curie temperature (T_C) is estimated to be 371 K.

A continuous magnetic phase transition exhibits critical behavior of different thermodynamic variables, governed by the critical fluctuation. The critical behavior is characterized by a set of static critical exponents. The values of these exponents depend only on the symmetry of the order parameter and the lattice dimensionality of the system, resulting in different universality classes of the continuous phase transition in uniform FMs. In the vicinity of T_C, the spin-spin correlation length (ξ) diverges as $\xi = \xi_0|(T - T_C)/T_C|^{-\nu}$, which leads to universal scaling laws for the spontaneous magnetization, $M_S(0, T)$, and inverse initial susceptibility, $\chi_0^{-1}(0, T)$. $M_S(0, T)$ below T_C, $\chi_0^{-1}(0, T)$ above T_C, and the magnetization isotherm $M(H, T_C)$ at T_C are characterized by a set of static critical exponents β, γ, and δ, respectively. These exponents are defined as follows [26]:

$$M_S(0, T) = [M_S(0)](-\varepsilon)^{\beta}, \quad \varepsilon < 0, \tag{1}$$

$$\chi_0^{-1}(0, T) = \left[\frac{H_0}{M_S(0)}\right](\varepsilon)^{\gamma}, \quad \varepsilon > 0, \tag{2}$$

$$M(H, T_C) = D(H)^{1/\delta}, \quad \varepsilon = 0, \tag{3}$$

where $\varepsilon = \frac{T - T_C}{T_C}$ is the reduced temperature, and $M_S(0)$, $\frac{H_0}{M_S(0)}$, and D are the critical amplitudes. The scaling theory predicts that in the close vicinity of the phase transition, the magnetic equation of state for the system can be expressed as

$$M(H, \varepsilon) = |\varepsilon|^{\beta} f_{\pm}\left[\frac{H}{|\varepsilon|^{(\gamma+\beta)}}\right], \tag{4}$$

where f_+ and f_- are regular functions for temperature above and below T_C, respectively. In terms of the renormalized magnetization, $m \equiv |\varepsilon|^{-\beta} M(H, \varepsilon)$, and the renormalized field, $h \equiv |\varepsilon|^{-(\gamma+\beta)} H$, the above scaling equation can be rewritten as

$$m = f_{\pm}(h). \tag{5}$$

The above equation implies that for the right choice of β, γ, and ε, the m versus h isotherms will fall onto two separate branches of the scaling function: f_+ for isotherms above T_C and f_- for isotherms below T_C. This is also an important criterion to check whether the set of critical exponents are the same below and above T_C.

To characterize the FM-to-PM phase transition in the present system, a series of magnetization isotherms, as shown in Fig. 3(a), has been measured in the vicinity of the approximate Curie temperature 371 K determined from the inset of Fig. 2. To test whether the framework of the Landau mean-field theory of the magnetic phase transition holds for Co$_2$TiGe, we have constructed the conventional Arrott plot [27] of M^2 versus H/M isotherms as shown in Fig. 3(b). For the mean-field values of the critical exponents ($\beta = 0.5$ and $\gamma = 1$), the Arrott plot should generate a set of parallel straight lines, and the one that passes through the origin of the plot corresponds to the isotherm at the exact critical temperature. However, the Arrott plot for Co$_2$TiGe does not constitute a set of parallel straight lines and shows significant nonlinearity with downward curvature even at high magnetic fields. Therefore, the Landau mean-field theory fails to describe the phase transition in Co$_2$TiGe and suggests the presence of significant critical fluctuations. According to Banerjee's criterion
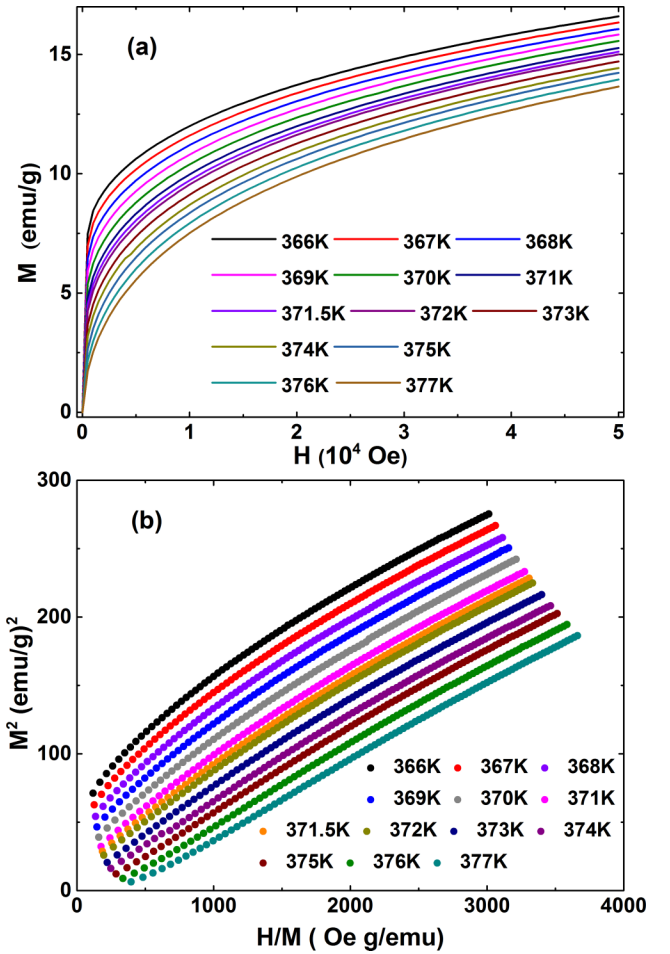

FIG. 3. (a) Isothermal magnetization (M vs H) as a function of magnetic field measured around T_C. (b) Arrott plot of isotherms measured in the vicinity of T_C.

[28], the positive values of the slope of the curves in the Arrott plot indicate the second-order nature of the phase transition. In Fig. 3(b), the M^2 versus H/M isotherms show downward curvature for $T < 371.5$ K and subtle upward curvature at low field for $T > 371.5$ K. But the slopes remain positive for all the isotherms, and thereby confirm the second-order FM-to-PM phase transition in Co$_2$TiGe.

To determine the true critical exponents, we have reanalyzed the magnetization isotherms using the modified Arrott plot [29] method, which is based on the following Arrott-Noakes equation of state:

$$(H/M)^{1/\gamma} = a\left(\frac{T - T_C}{T_C}\right) + bM^{1/\beta}. \tag{6}$$

Here, a and b are constants. The critical exponents predicted for the three-dimensional (3D) system by theoretical models such as the 3D Heisenberg ($\beta = 0.365$, $\gamma = 1.386$), the 3D XY ($\beta = 0.345$, $\gamma = 1.316$), and the 3D Ising ($\beta = 0.325$, $\gamma = 1.24$) models have been used to construct modified Arrott plots as shown in Figs. 4(a), 4(b) and 4(c), respectively. One can see from Figs. 4(a)–4(c) that in the high-field region, the constructions show quasistraight lines, which appear to be parallel to each other. To determine which one among
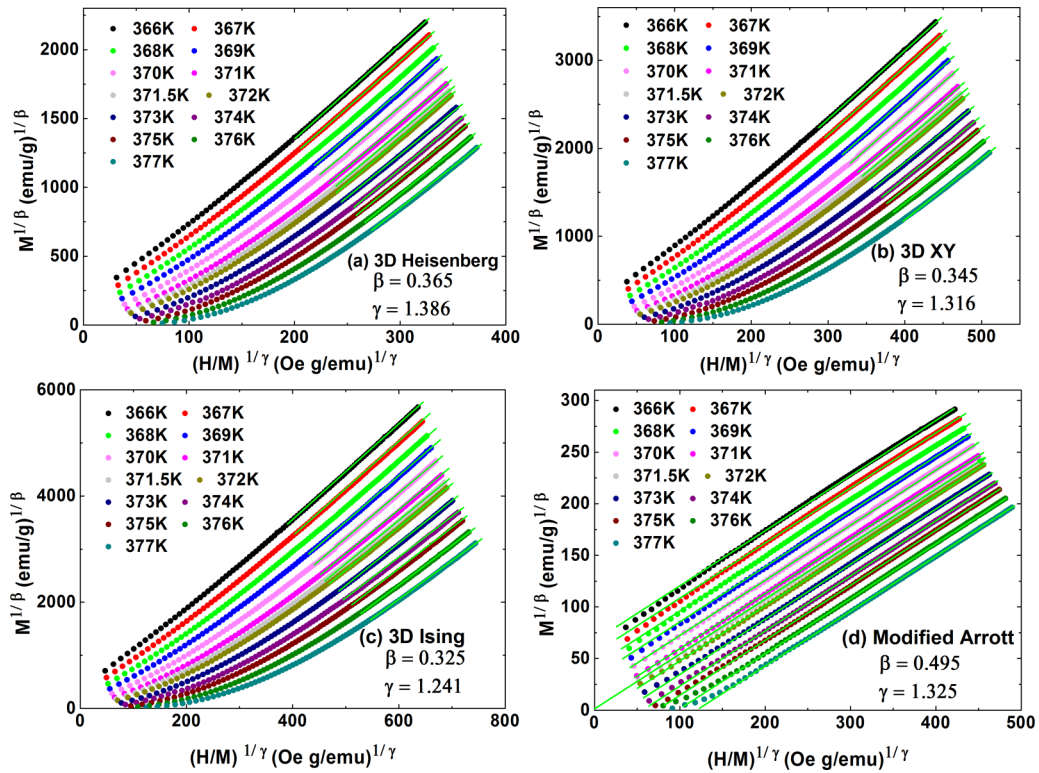
FIG. 4. Modified Arrott plot of isotherms for $366 \leqslant T \leqslant 377$ K, with the parameters of (a) the 3D Heisenberg model, (b) the 3D *XY* model, and (c) the 3D Ising model. (d) Modified Arrott plot of isotherms with $\beta = 0.495$ and $\gamma = 1.325$. Solid lines are the linear fits to the isotherms in the high-field regions.

these three models generates the best modified Arrott plot with parallel isotherms, we have compared the slope of these straight lines (obtained from the linear fits to the isotherms in the high-field region) to that obtained for the isotherm at $T \simeq T_C$ for each modified Arrott plot. Here, the slope is defined as $S(T) = dM^{1/\beta}/d(H/M)^{1/\gamma}$. The obtained normalized slopes, NS $= S(T)/S(T_C)$, for each model have been plotted as a function of temperature in Fig. 5. It is evident that the values of the NS deviate progressively from the ideal value
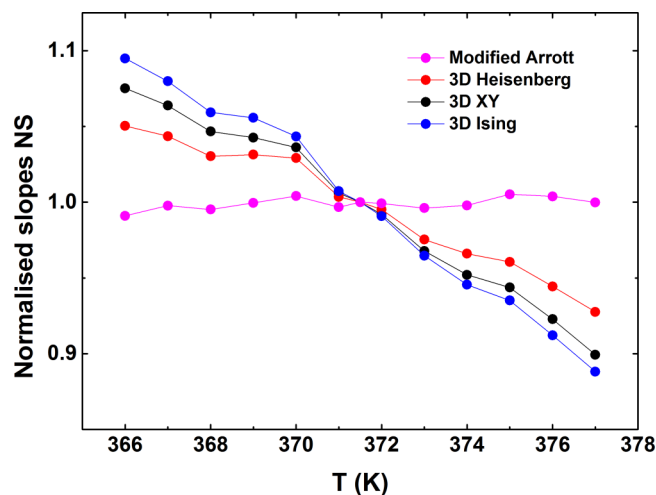

FIG. 5. Temperature dependence of the normalized slopes, NS $= S(T)/S(T_C)$, obtained from Figs. 4(a)–4(d).

of 1 both below and above T_C. However, among these three models, the deviation is minimum for the 3D Heisenberg model. Therefore, the modified Arrott plot corresponding to the 3D Heisenberg model [Fig. 4(a)] has been used for further refinement of the exponents β and γ using a rigorous iterative method as described below.

In Fig. 4(a), the intercepts of the linear fits (to the isotherms in high-field region), with the axes $M^{1/\beta}$ and $(H/M)^{1/\gamma}$, give reliable values of $M_S(0, T)$ and $\chi_0^{-1}(0, T)$, respectively. The power-law fits to the data following Eqs. (1) and (2) yield new values of the exponents β and γ, which are used to construct a new modified Arrott plot. During the fitting, T_C was varied to get the best-fit results. From this plot, new $M^{1/\beta}$ and $(H/M)^{1/\gamma}$ are obtained by linear fits to the isotherms at the high-field region. So we get a new set of β and γ. This procedure is repeated to achieve self-consistency, i.e., when the new values of the critical exponents become almost equal to the values before that iteration.

The final modified Arrott plot, constructed using $\beta = 0.495$ and $\gamma = 1.325$, is shown in Fig. 4(d). The normalized slopes of the linear fits to the isotherms of this modified Arrott plot are also shown in Fig. 5. Here, one can see that both above and below T_C, the normalized slope is close to 1, implying that all the isotherms form parallel straight lines with the isotherm at $T = 371.5$ K, which almost passes through the origin of the plot. Thus, the more accurate value of T_C is estimated to be 371.5 K. In the low-field region, the small curvatures in the isotherms of Fig. 4(d) are due to the reorientation of the domains at low magnetic fields. The temperature dependences of $M_S(0, T)$ and $\chi_0^{-1}(0, T)$, which are obtained from Fig. 4(d),
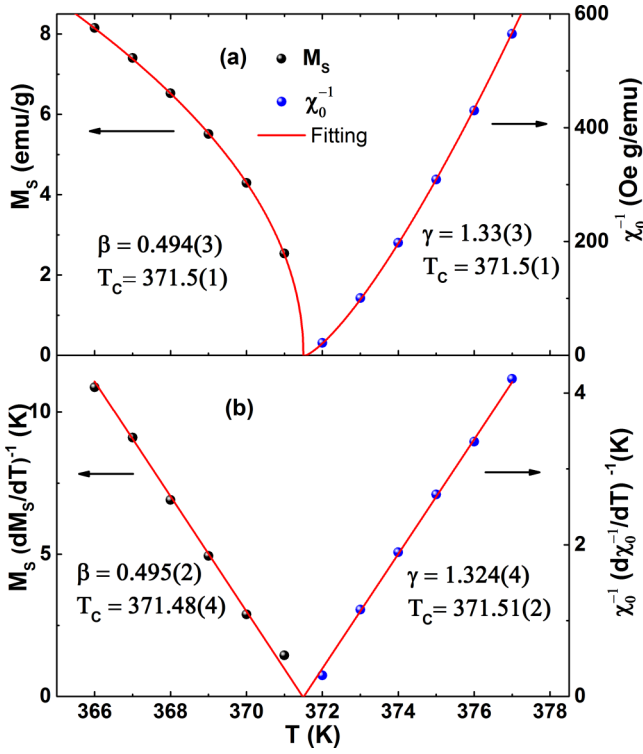
FIG. 6. (a) Temperature variations of M_S and χ_0^{-1} along with the fits (solid lines) following Eqs. (1) and (2), which give the values of the exponents and T_C as mentioned in the plot. (b) Kouvel-Fisher plot of M_S and χ_0^{-1}. The exponents and T_C are obtained from the linear fits (solid lines) of the data.

are shown in Fig. 6(a). The power-law fit following Eq. (1) to the $M_S(0, T)$ data yields $\beta = 0.494(3)$ and $T_C = 371.5(1)$, and fitting of Eq. (2) to the $\chi_0^{-1}(0, T)$ data gives $\gamma = 1.33(3)$ and $T_C = 371.5(1)$. These values of the exponents and T_C are almost the same as that obtained from the modified Arrott plot [Fig. 4(d)]. Therefore, the estimated values of β, γ, and T_C are reliable and intrinsic.

Accurate values of the exponents as well as T_C can also be obtained using the Kouvel-Fisher technique [30]. According to this method, $M_S(\frac{dM_S}{dT})^{-1}$ versus T and $[\chi_0(\frac{d\chi_0^{-1}}{dT})]^{-1}$ versus
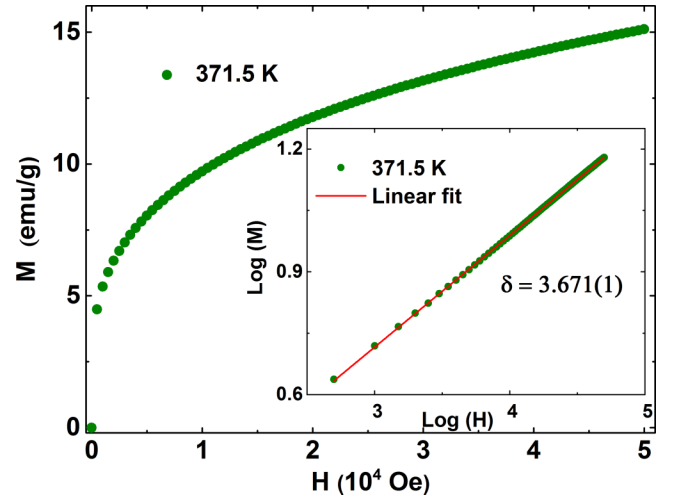

FIG. 7. Field dependence of the magnetization isotherm at $T_C = 371.5$ K for Co_2TiGe. The inset shows the same plot in log-log scale, where the solid line is the linear fit following Eq. (3) that gives the critical exponent δ as mentioned in the graph.

T should be straight lines with slopes $\frac{1}{\beta}$ and $\frac{1}{\gamma}$, respectively, and their intercepts on the T-axis give the value of T_C. The linear fits to these plots [shown in Fig. 6(b)] yield $\beta = 0.495(2)$, $T_C = 371.48(4)$ and $\gamma = 1.324(4)$, $T_C = 371.51(2)$.

The critical exponent δ can be obtained from the critical isotherms, i.e., the $M(H)$ isotherm at $T = T_C$ as well as from the Widom scaling relation [31]:

$$\delta = 1 + \frac{\gamma}{\beta}. \tag{7}$$

The $M(H)$ plot at $T = 371.5$ K is shown in Fig. 7 and the inset shows the same plot on the log-log scale. Following Eq. (3), from the inverse of the slope of the linear fit to the $\log(M)$ versus $\log(H)$ curve, we obtain $\delta = 3.671(1)$. Using the values of β and γ obtained from Figs. 6(a) and 6(b), the Widom scaling relation, Eq. (7), gives $\delta = 3.692$ and 3.675, respectively. These values of δ are very close to that obtained from the critical isotherms (Fig. 7). Hence the obtained values

TABLE I. Comparison of critical exponents of Co_2TiGe with earlier reports on itinerant uniform FM Ni, itinerant amorphous FM $Gd_{80}Au_{20}$, and different theoretical models. Abbreviation: modified Arrott plot (MAP), Kouvel-Fisher (KF), critical isotherm (CI), renormalization-group epsilon ($\epsilon' = 2\sigma - d$) expansion (RG-ϵ').

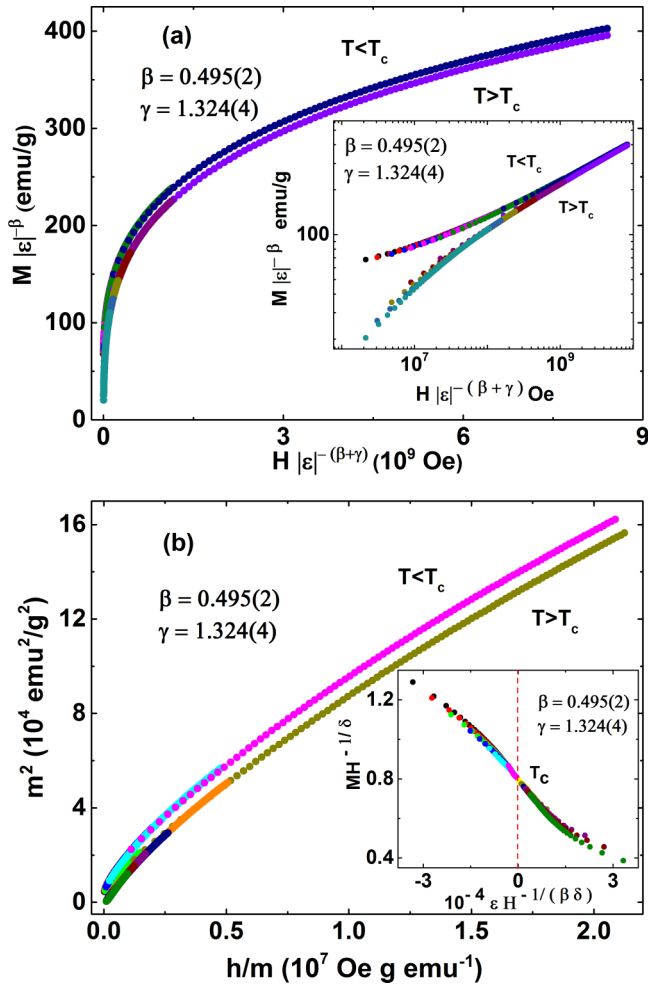| Material/Model	Ref.	Technique	T_C	β	γ	δ
Co_2TiGe	This work	MAP	371.5	0.495	1.325	3.677
	This work	KF	371.5(1)	0.495(2)	1.324(4)	3.675
	This work	CI				3.671(1)
Ni	[32]	KF		0.391(10)	1.314(16)	4.39(2)
$Gd_{80}Au_{20}$	[37]	KF		0.44(2)	1.29(5)	3.96(3)
Mean field	[26]	Theory		0.5	1	3
3D Heisenberg	[28,41]	Theory		0.365	1.386	4.8
3D XY	[28,42]	Theory		0.345	1.316	4.81
3D Ising	[28,42]	Theory		0.325	1.24	4.82
LR exchange: $J(r) = 1/r^{d+\sigma}$						
$d = 3, n = 3, \sigma = 1.88$	[43]	RG-ϵ'		0.393	1.32	4.36

FIG. 8. (a) Scaled magnetization as a function of the renormalized field for Co$_2$TiGe, indicating two separate branches of the scaling for isotherms below and above T_C. The inset shows the same plot in log-log scale. (b) The replotting of renormalized magnetization (m) and renormalized field (h) in the form of m^2 vs h/m. The inset shows the rescaling of the $M(H)$ isotherms by $MH^{-1/\delta}$ vs $H^{-1/(\beta\delta)}$, where all the data collapse on a single curve following Eq. (8).

of critical exponents and T_C are self-consistent and obey the Widom scaling relation very well.

The values of the critical exponents β, γ, and δ, obtained from various methods, are presented in Table I along with the theoretically predicted values for different models. From Table I, at a glance we see that the values of the exponents for the present system do not belong to any of the conventional universality classes. Therefore, we must check whether these exponents can generate the scaling equation of state as given by Eq. (5). In Fig. 8(a), scaled-m versus scaled-h has been plotted using the values of critical exponents β, γ, and T_C, calculated from the Kouvel-Fisher plot. The inset shows the same plot on log-log scale to expand the low-field region. From Fig. 8(a), it is clear that all the isotherms collapse onto two separate branches: one above T_C and another below T_C. The reliability of the values of the exponents and T_C is further verified by plotting m^2 versus h/m, as shown in Fig. 8(b). In this case, all the isotherms also fall on two independent

branches of the scaling function. Furthermore, in the vicinity of the transition, the scaling equation of state can be rewritten in another form,

$$\frac{H}{M^\delta} = k\left(\frac{\varepsilon}{H^{1/\beta}}\right), \tag{8}$$

where k is a regular scaling function. The scaling Eq. (8) implies that all the isotherms now collapse onto a single curve. Following Eq. (8), we have plotted $MH^{-1/\delta}$ versus $\varepsilon H^{-1/\beta\delta}$ in the inset of Fig. 8(b). The inset shows that all the experimental data fall on a single curve passing through T_C, which is located at zero on the horizontal axis of the plot. Therefore, the scaling behavior shown in Figs. 8(a) and 8(b) implies that all the interactions in the vicinity of T_C get properly renormalized and the set of critical exponents are the same below and above T_C for the present compound.

The static critical exponents for Co$_2$TiGe, obtained from the aforementioned rigorous methods, obey the scaling relation and the scaling equation of state. Therefore, these exponents truly characterize the critical behavior in the compound. However, a comparison of these exponents with that predicted by different theoretical models for the 3D system confirms that estimated critical exponents for Co$_2$TiGe do not belong to any conventional universality class and fall between the values predicted by the 3D Heisenberg model and the mean-field theory. It should be mentioned that the asymptotic critical exponents, which are temperature-independent in the asymptotic critical regime, truly characterize the critical behavior in a material belonging to a universality class. Usually, the asymptotic critical regime is $|\varepsilon| \leqslant 10^{-2}$ for homogeneous magnets and slightly larger for disordered and amorphous systems [32]. The reduced temperature range, used to derive the critical exponents for Co$_2$TiGe, is $1.3 \times 10^{-3} \leqslant |\varepsilon| \leqslant 1.4 \times 10^{-2}$. Therefore, we have performed the above analysis in the asymptotic critical regime. Indeed, we noticed that the estimated effective critical exponents (β_{eff} and γ_{eff}) remain almost the same in the studied reduced temperature range [32,33]. The observed discrepancy from the 3D Heisenberg values may result from two possibilities: (i) exchange interaction of extended-type, i.e., interactions beyond the nearest neighbor, and (ii) magnetic inhomogeneity in the system. Hence, it is necessary to understand the nature as well as the range of interaction in this material. Renormalization-group analysis has shown that the isotropic long-range dipolar interaction can drive a crossover toward mean-field exponents at a certain value ε_{co} of the reduced temperature, which depends on the strength of the dipolar interactions [32,34,35]. The analysis also shows that the new crossover exponents are only slightly different from the Heisenberg ones and shifted toward the mean-field values. The general theory of the crossover phenomenon gives the crossover temperature as $\varepsilon_{\text{co}} \approx g_d^{1/\phi_d}$, where g_d is the strength of the dipolar interaction and ϕ_d is the crossover exponent [36]. g_d can be estimated from $g_d \approx \frac{0.87}{T_C}\frac{p^2\theta}{v}$ [34–36], where $p = g\sqrt{S(S+1)}$, θ is a correction factor, and v is the elementary cell volume in Å^3. For the present material, $v = 196.93$ Å^3 and for spin $S = 1/2$, θ can be taken as 0.68 [36]. Using these parameters, we get $g_d = 2.426 \times 10^{-5}$ for Co$_2$TiGe. Taking the crossover exponent ϕ_d as the Heisenberg exponent $\gamma = 1.386$, we estimate the

crossover temperature to be $\varepsilon_{co} = 4.78 \times 10^{-4}$ [32,36]. Only for $\varepsilon \ll \varepsilon_{co}$ does the dipolar interaction result in a new regime with exponents shifted toward mean-field values. Therefore, the isotropic dipolar picture is not consistent with the present scenario since the estimated ε_{co} for Co_2TiGe is well below the investigated asymptotic critical regime, $1.3 \times 10^{-3} \leqslant |\varepsilon| \leqslant 1.4 \times 10^{-2}$. However, the extended type of interaction can also arise from isotropic exchange interaction between spins involving itinerant electrons that decays spatially as $J(r) \propto 1/r^{d+\sigma}$, where d is the effective dimensionality of the spin interaction and σ is a measure of the range of the exchange interaction [20]. In a 3D system with isotropic spins, the Heisenberg model is realized for $\sigma > 2$ such that $J(r)$ decreases with r faster than r^{-5}. Mean-field exponents are realized when $J(r) \propto r^{-m}$ with $m < 4.5$. For $3/2 \leqslant \sigma \leqslant 2$, the system belongs to a different class with critical exponents that take intermediate values depending on σ. Given the dimensionality of lattice (d) and spin (n), σ can be estimated using the renormalization-group approach, which gives [20]

$$\gamma = 1 + \frac{4}{d}\left(\frac{n+2}{n+8}\right)\Delta\sigma + \frac{8(n+2)(n-4)}{d^2(n+8)^2}$$
$$\times \left\{1 + \frac{2G\left(\frac{d}{2}\right)(7n+20)}{(n-4)(n+8)}\right\}\Delta\sigma^2, \qquad (9)$$

where $\Delta\sigma = (\sigma - \frac{d}{2})$ and $G(\frac{d}{2}) = 3 - \frac{1}{4}(\frac{d}{2})^2$. Using Eq. (9), for $d : n = 3 : 3$ and $\sigma = 1.88$, we have obtained the experimentally estimated value of $\gamma = 1.32$. However, for $\sigma = 1.88$, scaling relations [26] yield $\beta = 0.393$, which deviates from the 3D Heisenberg value toward the mean-field one but not as much as observed experimentally (Table I). The value of σ suggests the extended nature of the exchange interaction, which could be due to the presence of RKKY-type long-range interaction between spins involving itinerant electrons as argued by others and discussed earlier [11]. The asymptotic critical exponents for uniform ferromagnet Ni (Table I) are also shifted toward the mean-field values, and the shift is attributed to a crossover to the fixed-point corresponding to the isotropic long-range exchange interactions [32]. But, in Co_2TiGe, the large deviation in the value of the critical exponent β from the 3D Heisenberg value cannot be explained only on the basis of the extended nature of the exchange interaction. It should be mentioned that the mean-field-like values of β have been reported for several magnetically

inhomogeneous systems [37–39]. The amorphous FM $Gd_{80}Au_{20}$ also shows unusual values of the critical exponents (Table I), all being largely shifted toward the mean-field values, and they are attributed to the dilution model for inhomogeneous FMs [37,40]. Magnetic inhomogeneities may lead to critical phenomena that could not be described on the basis of existing universality classes. However, unlike inhomogeneous FMs, the critical exponent γ shows quite a small shift toward the mean-field one for Co_2TiGe. Thus, the obtained values of the critical exponents in Co_2TiGe cannot be accounted for by the magnetic inhomogeneity alone. Therefore, we believe that the observed unconventional critical exponents in Co_2TiGe comply with the complex nature of exchange interactions, involving both the short-range and beyond nearest-neighbor spin-spin interactions, and they also suggest some magnetic inhomogeneity in the system.

IV. CONCLUSION

To summarize, we have comprehensively studied the critical behavior in the half-metallic full-Heusler ferromagnet Co_2TiGe in the vicinity of the ferromagnetic-to-paramagnetic phase transition at $T_C = 371.5$ K. Although magnetic Heusler alloys are regarded as an ideal local-moment system and their spin-spin interactions are modeled by a Heisenberg Hamiltonian, we observe a significant deviation in the values of critical exponents from the 3D Heisenberg toward the mean-field ones in Co_2TiGe. In particular, the value of the critical exponent β is very close to the mean-field one. This implies diminished critical spin-fluctuation in the vicinity of the transition temperature, which could be due to the presence of exchange interactions beyond the nearest-neighbor spin as well as magnetic inhomogeneity in the compound. The results are consistent with the recently argued fact that both the short-range direct exchange coupling between nearest-neighbor spins and the indirect coupling between further-neighbor spins mediated by the long-range RKKY interaction stabilize the long-range ferromagnetic ordering. The present study provides experimental evidence of the complex nature of exchange interactions in the Co_2-based full Heusler ferromagnet, which does not belong to any known universality class predicted by theory.

[1] F. Heusler, Verh. Deutsch. Phys. Ges. **5**, 219 (1903).

[2] P. J. Webster, J. Phys. Chem. Solids **32**, 1221 (1971).

[3] P. J. Webster and K. R. A. Ziebeck, J. Phys. Chem. Solids **34**, 1647 (1973).

[4] A. Hamzic, R. Asomoza, and I. A. Campbell, J. Phys. F **11**, 1441 (1981)

[5] D. C. Price, J. Phys. F **8**, 933 (1978).

[6] J. Kübler, A. R. Williams, and C. B. Sommers, Phys. Rev. B **28**, 1745 (1983).

[7] J. L. Morán-Lópeza, R. Rodriguez-Albab, and F. Aguilera-Granjab, J. Magn. Magn. Mater. **131**, 417 (1994).

[8] Y. Kurtulus, R. Dronskowski, G. D. Samolyuk, and V. P. Antropov, Phys. Rev. B **71**, 014425 (2005).

[9] E. Sasioglu, L. M. Sandratskii, P. Bruno, and I. Galanakis, Phys. Rev. B **72**, 184415 (2005).

[10] J. Thoene, S. Chadov, G. Fecher, C. Felser, and J. Kübler, J. Phys. D **42**, 084013 (2009).

[11] S. Trudel, O. Gaier, J. Hamrle, and B. Hillebrands, J. Phys. D **43**, 193001 (2010).

[12] R. A. de Groot, F. M. Mueller, P. G. van Engen, and K. H. J. Buschow, Phys. Rev. Lett. **50**, 2024 (1983).

[13] I. Galanakis, P. H. Dederichs, and N. Papanikolaou, Phys. Rev. B **66**, 174429 (2002).

[14] C. Chappert, A. Fert, and F. Nguyen Van Dau, Nat. Mater. **6**, 813 (2007).

[15] G. Chang, S. Xu, H. Zheng, B. Singh, C. Hsu, G. Bian, N. Alidoust, I. Belopolski, D. S. Sanchez, S. Zhang, H. Lin, and M. Z. Hasan, Sci. Rep. **6**, 38839 (2016).

[16] J. Barth, G. H. Fecher, B. Balke, S. Ouardi, T. Graf, C. Felser, A. Shkabko, A. Weidenkaff, P. Klaer, H. J. Elmers, H. Yoshikawa, S. Ueda, and K. Kobayashi, Phys. Rev. B **81**, 064404 (2010).

[17] N. D. Telling, P. S. Keatley, G. van der Laan, R. J. Hicken, E. Arenholz, Y. Sakuraba, M. Oogane, Y. Ando, K. Takanashi, A. Sakuma, and T. Miyazaki, Phys. Rev. B **78**, 184438 (2008).

[18] P. Klaer, M. Kallmayer, C. G. F. Blum, T. Graf, J. Barth, B. Balke, G. H. Fecher, C. Felser, and H. J. Elmers, Phys. Rev. B **80**, 144405 (2009).

[19] K. Miyamoto, A. Kimura, K. Iori, K. Sakamoto, T. Xie, T. Moko, S. Qiao, M. Taniguchi, and K. Tsuchiya, J. Phys.: Condens. Matter **16**, S5797 (2004).

[20] M. E. Fisher, S. Ma, and B. G. Nickel, Phys. Rev. Lett. **29**, 917 (1972).

[21] L. Bainsla and K. G. Suresh, Curr. Appl. Phys. **16**, 68 (2016).

[22] B. Balke, S. Wurmehl, G. H. Fecher, C. Felser, M. C. M. Alves, F. Bernardi, and J. Morais, Appl. Phys. Lett. **90**, 172501 (2007).

[23] G. E. Bacon and J. S. Plant, J. Phys. F **1**, 524 (1971).

[24] B. Ravel, M. P. Raphael, V. G. Harris, R. Ramesh, and V. Saraf, Appl. Phys. Lett. **81**, 2812 (2002).

[25] J. Barth, G. H. Fecher, B. Balke, T. Graf, A. Shkabko, A. Weidenkaff, P. Klaer, M. Kallmayer, H.-J. Elmers, H. Yoshikawa, S. Ueda, K. Kobayashi, and C. Felser, Philos. Trans. R. Soc. A **369**, 3588 (2011).

[26] H. Eugene Stanley, *Introduction to Phase Transitions and Critical Phenomena* (Oxford University Press, New York, 1971).

[27] A. Arrott, Phys. Rev. **108**, 1394 (1957).

[28] S. K. Banerjee, Phys. Lett. **12**, 16 (1964).

[29] A. Arrott and J. Noakes, Phys. Rev. Lett. **19**, 786 (1967).

[30] J. S. Kouvel and M. E. Fisher, Phys. Rev. **136**, A1626 (1964).

[31] B. Widom, J. Chem. Phys. **43**, 3898 (1965); **41**, 1633 (1964).

[32] M. Seeger, S. N. Kaul, H. Kronmüller, and R. Reisser, Phys. Rev. B **51**, 12585 (1995).

[33] P. D. Babu and S. N. Kaul, J. Phys.: Condens. Matter **9**, 7189 (1997).

[34] A. Aharony and M. E. Fisher, Phys. Rev. B **8**, 3323 (1973)

[35] M. E. Fisher and A. Aharony, Phys. Rev. Lett. **30**, 559 (1973).

[36] K. Ried, D. Köhler, and H. Kronmüller, J. Magn. Magn. Mater. **116**, 259 (1992).

[37] S. J. Poon and J. Durand, Phys. Rev. B **16**, 316 (1977).

[38] N. Khan, P. Mandal, K. Mydeen, and D. Prabhakaran, Phys. Rev. B **85**, 214419 (2012).

[39] R. Venkatesh, M. Pattabiraman, S. Angappane, G. Rangarajan, K. Sethupathi, J. Karatha, M. Fecioru-Morariu, R. M. Ghadimi, and G. Güntherodt, Phys. Rev. B **75**, 224415 (2007).

[40] H. Müller-Krumbhaar, J. Phys. C **9**, 345 (1976).

[41] M. Campostrini, M. Hasenbusch, A. Pelissetto, P. Rossi, and E. Vicari, Phys. Rev. B **65**, 144520 (2002).

[42] J. C. Le Guillou and J. Zinn-Justin, Phys. Rev. B **21**, 3976 (1980).

[43] M. E. Fisher, Rev. Mod. Phys. **46**, 597 (1974).